Powder Technology 311 (2017) 514–521

Contents lists available at ScienceDirect

Powder Technology

journal homepage: www.elsevier.com/locate/powtec

Research on bead width and penetration depth of multicomponent flux-aided arc welding of grade 316 L stainless steel

Kuang-Hung Tseng *, Nai-Shien Wang

Institute of Materials Engineering, National Pingtung University of Science and Technology, Pingtung 91201, Taiwan

ARTICLE INFO

Article history:
Received 4 September 2016
Received in revised form 30 January 2017
Accepted 2 February 2017
Available online 04 February 2017

Keywords:
Multicomponent flux
Bead width
Penetration depth
Plasma arc welding
Gas tungsten arc welding

ABSTRACT

This work investigated the influence of a multicomponent flux on the bead width and penetration depth of grade 316 L stainless steels subjected to gas tungsten arc welding (GTAW) and plasma arc welding (PAW). Powdered oxide/fluoride mixture mixed with single or multicomponent solvent was used as the flux. This paper also discusses the potential mechanism leading to the increase in joint-penetrating capability with use of the flux during PAW, and it compares results obtained with flux-aided GTAW (F-GTAW). The results indicate that a 60% methanol/40% water or a 40% acetone/60% water is an appropriate solvent mixture for mixing with the multicomponent powders. Compared with GTAW, which formed a shallow and wide profile, F-GTAW, PAW, or flux-aided PAW (F-PAW) formed a deep and narrow profile. F-GTAW produced a weld cross-sectional profile similar to that produced by PAW. The influence of the flux on the geometry of the PA weld was not as pronounced as that on the geometry of the GTA weld. The results of our study suggest that a 30% SiO_2, 25% TiO_2, 20% ZnO, 12% NiO, 5% MgO, 3% Cu_2O and 5% FeF_2 flux not only substantially improves the joint penetration of the GTA weld, but it also produces a PA weld with a more uniform cross-sectional profile.

1. Introduction

Arc welding is a type of fusion welding that uses a welding power supply in order to create an electric arc between an electrode and the workpiece. The arc welding is commonly used in both home workshops and factories because of the low cost of its installation and maintenance. Arc welding can be divided into methods that use non-consumable electrodes and consumable electrodes [1]. Arc welding that uses a non-consumable electrode generally has an arc efficiency lower than that of arc welding using a consumable electrode [2]. In the GTAW, the heat required for welding is generated by a cone-shaped arc established between the non-consumable electrode and the workpiece. The molten metal is shielded from atmospheric contamination by an inert gas. The primary drawback of the GTAW is its productivity; both its travel speed and deposition rate are relatively low. PAW is a variation of GTAW in which the non-consumable electrode is positioned within the body of the torch itself [3]. With such positioning, the plasma arc is separated from the shielding gas envelope. A high-temperature plasma is then forced through a small-bore orifice to produce a cylinder-shaped arc. Compared with the cone-shaped arc formed in GTAW at the same current level, the cylinder-shaped arc formed in PAW has a lower divergence angle and a higher energy density.

Developments in arc welding are strongly motivated by the need for increasing productivity without sacrificing the quality of the welded joint. The use of a flux in arc welding is a notable innovation that can significantly increase productivity [4,5]. Here, the flux is in the form of compound powder that is mixed with a carrier solvent to form a paste-like mixture [6,7]. Flux-aided arc welding (F-AW) is an advanced welding technique in which a thin flux layer is painted onto the surface of the base metal to be welded, and then a single-pass operation is performed in order to increase the joint penetration of the weld [8,9]. The GTAW using a flux is the most common variant of F-AW technique. The E.O. Paton Electric Welding Institute (Kiev, Ukraine) first proposed the use of F-GTAW [4,10,11]. The advancement of F-GTAW in the former Soviet Union has led to its use in a wide range of industries, including aerospace, automotive, military, power generation and chemical industries [12]. Furthermore, both the Edison Welding Institute (Ohio, United States) and The Welding Institute (Cambridge, United Kingdom) evaluated the technical feasibility of and set forth the operating procedure for F-GTAW. F-GTAW can significantly enhance productivity; therefore, there has been a great deal of interest in the research and development of this technique [13].

In contrast to the substantial amount of research into F-GTAW technique, studies on the F-PAW technique are limited. Fluxes for these techniques in industrial applications have recently become commercially available [14]. The flux ingredient is a critical factor in increasing the penetration depth and reducing the bead width of the weld [6,15]. Most research, however, remains focused on the use of

* Corresponding author at: No. 1, Hseuhfu Rd., Neipu, Pingtung 91201, Taiwan.
E-mail address: tkh@mail.npust.edu.tw (K.-H. Tseng).

http://dx.doi.org/10.1016/j.powtec.2017.02.005
0032-5910/

Table 1
Chemical composition of grade 316 L stainless steel (wt%).

C	Si	Mn	P	S	Cr	Ni	Mo	Fe
0.026	0.51	1.28	0.027	0.015	16.9	11.1	2.09	bal.

the single-component fluxes. The open literature has limited data on multicomponent fluxes, despite that this information is critical to determinations of the joint-penetrating capability with use of the flux in F-AW. The selection of a suitable carrier solvent for mixing with the flux powder is very important to producing a high-quality coating. The relationship between the carrier solvent and the flux powder has thus been investigated. The present work used a multicomponent flux developed by the National Pingtung University of Science and Technology (NPUST), Taiwan, in order to investigate the effects of the flux ingredient on the bead width and penetration depth of a stainless steel weld. This paper also discusses the integrated mechanism behind the increase in joint-penetrating capability in PAW using a flux, as well as compares the results with those obtained using the F-GTAW. Ultimately, knowledge of these sciences may contribute to the development of new multicomponent fluxes that are suitable for both GTAW and PAW of stainless steels.

2. Experimental details

An annealed grade 316 L stainless steel plate with 6 mm thickness was the metal to be welded. Table 1 shows the chemical composition of grade 316 L stainless steel as received for this study. Grade 316 L is a molybdenum-containing austenitic stainless steel. Compared with grade 304 L stainless steel, grade 316 L stainless steel has better overall resistance to corrosion, especially pitting and crevice corrosion in chloride-containing environments. The stainless steel plates were machined into specimens with dimensions of 150 mm × 150 mm for the welding trials.

A 30% SiO_2, 25% TiO_2, 20% ZnO, 12% NiO, 5% MgO, 3% Cu_2O and 5% FeF_2 flux was developed by the NPUST (Pingtung, Taiwan). The powdered oxide/fluoride mixture has an average particle size of 74 μm. Prior to welding, 1000 mg of flux powder was mixed with 1.8 ml of carrier solvent, and the resulting mixture was stirred with a glass rod in a beaker until a paste-like consistency was attained. The paste-like flux was subsequently coated onto the specimen with a flat brush. Upon evaporation of the carrier solvent, the flux layer remained attached to the surface of the specimen. Fig. 1 shows the preparation process of the paste-like flux. In the present work, the flux layer had a width and length of 10 mm and 150 mm, respectively, and the weight of flux layer per unit area was 2.3 ± 0.1 mg/cm^2.

A constant-current power source together with a semi-automatic operation system was used in all welding trials. A machine-mounted torch having a 1.5% lanthanated tungsten electrode was moved along a linear guideway perpendicular to the centerline of the specimen. High-purity argon was used as shielding gas and orifice gas. An autogenous single-pass welding operation was performed to produce a bead-on-plate weld. Table 2 lists the welding conditions used in the GTAW and PAW trials. Prior to welding, the included angle of the electrode tip was ground, and the electrode gap was measured for each trial to ensure that all welding trials were performed under the same conditions. During welding, a digital video recorder was used to monitor the arc voltage values, and a charge-coupled device detector was used to collect the welding arc images.

Table 2
Welding conditions used in GTAW and PAW trials.

Welding conditions	Welding trial	
	GTAW	PAW
Welding current	120–190 A	90–130 A
Travel speed	150 mm/min	150 mm/min
Electrode diameter	ϕ3.2 mm	ϕ4.8 mm
Included angle of electrode tip	60°	30°
Electrode gap distance	3 mm	5 mm
Nozzle stand-off distance	8 mm	3 mm
Flow rate of shielding gas	15 l/min	15 l/min
Flow rate of orifice gas	–	0.8 l/min

After the welding trials, the metallographic samples were cross-sectioned perpendicular to the welding direction and mounted in a resin, which was then ground to a size of 1200 grit with SiC sandpaper, and then polished to a size of 0.05 μm with Al_2O_3 suspensions, and electrolytic etched with a 10% aqueous oxalic acid. The profile of the weld was photographed using a stereo microscope, and its dimension was measured using a toolmaker's microscope. Moreover, an oxygen/nitrogen/hydrogen elemental analyzer was used to measure the oxygen concentration in the weld.

3. Results and discussion

The aim of the present work was to investigate the effect of a multicomponent flux on the bead width and penetration depth of stainless steels subjected to GTAW and PAW. The potential mechanisms leading to the increase in joint-penetrating capability with use of the flux in both GTAW and PAW are discussed here. The effects of carrier solvents on the coverability and volatility of the flux layers were also investigated.

3.1. Effect of single solvent on coverability and volatility of flux layer

Fig. 2 shows the coverability of the flux layer obtained with various single solvents. In this trial, 1000 mg of multicomponent powder was mixed with 1.8 ml of either pure water (100% W), pure methanol (100% M), or pure acetone (100% A) solvent to form a paste-like flux. Table 3 lists the physical properties of water, methanol and acetone [4]. The results indicate that the flux layer formed by the powder mixed with 100% W exhibited the best coverability, followed by the layers formed using 100% M and 100% A. This trend is due to the higher viscosity of water compared with that of methanol and acetone. For F-AW, the volatility of the carrier solvent must also be taken into consideration. Table 4 shows the volatility of the flux layer obtained with various single solvents. The data show that the powder mixed

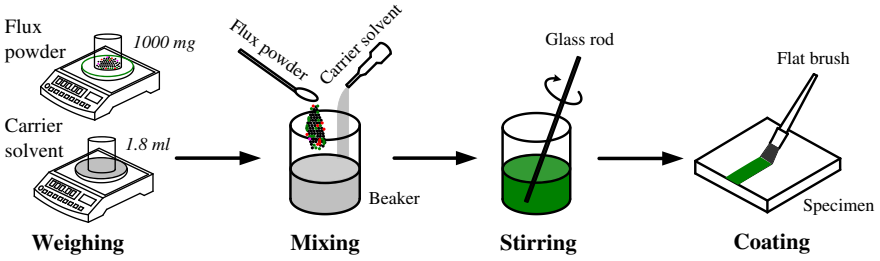

Fig. 1. Preparation process of paste-like flux.

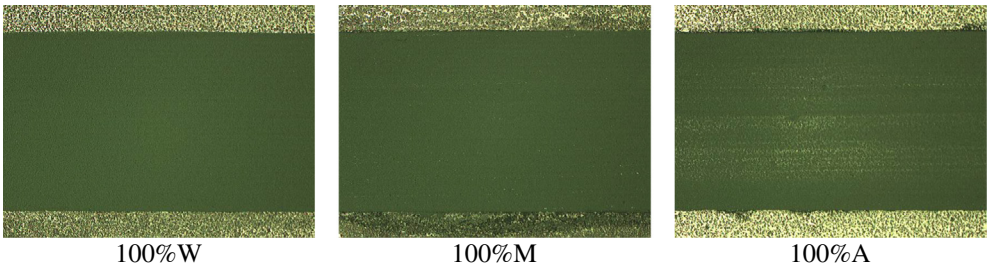

Fig. 2. Coverability of flux layer obtained with various single solvents.

with 100% A exhibited the highest volatility among all of the flux layers, followed by the volatilities observed with 100% M and 100% W. This trend is due to the much higher vapor pressure of acetone compared with that of methanol and water. According to the results of this trial, a single solvent cannot provide a flux layer with good coatability.

3.2. Effect of multicomponent solvent on coverability and volatility of flux layer

Fig. 3 shows the coverability of the flux layer obtained with various multicomponent solvents. In this trial, 1000 mg of multicomponent powder was mixed with 1.8 ml of either methanol/water (M/W), acetone/water (A/W), or methanol/acetone (M/A) to form a paste-like flux. The results indicate that the powder mixed with the M/W solvent exhibited the best coverability among the fluxes, followed by the coverabilities obtained with A/W and M/A solvents. The 40% A/60% W or 20% A/80% W solvents could be used to obtain a flux layer with good coverability. Table 5 shows the volatility of the flux layer obtained with various multicomponent solvents. The data show that the powder mixed with the M/A exhibited the highest volatility among the flux layers, followed by the volatilities of the layers made with A/W and M/W. On the basis of the relative coverabilities (major factor) and volatilities (minor factor) of the flux layers, we conclude that a 60% M/40% W or a 40% A/60% W is an appropriate solvent mixture for mixing with the multicomponent powders. The advantage of 60% M/40% W or 40% A/60% W over 100% W is its potential to improve the volatility of the flux layer. Moreover, 60% M/40% W or 40% A/60% W can enhance the coverability of the flux layer in comparison with that achieved using 100% A.

3.3. Research on bead width and penetration depth of F-GTA and F-PA welds

The quality of the welded joint is largely determined by the weld geometry. As both GTAW and PAW use a constant-current power source, the welding current is the most important parameter that affects the geometry of the resultant weld. This is because the welding current has significant effects on the induced Lorentz force, which is the driving force for fluid flow in an electric arc. In the present work, the effects of the welding current on the bead width and penetration depth were determined by using currents between 120 A and 190 A for GTAW and F-GTAW; currents between 90 A and 130 A were used for PAW and F-PAW. Fig. 4 shows the effect of the welding current on the bead width of the weld. A graph for the bead width of the GTA weld has a steep slope, whereas the graphs for the bead width of the F-GTA, PA and F-PA welds have gradual slopes. Fig. 5 shows the effect of the welding current on the penetration depth of the weld. A graph for the penetration depth of the GTA weld has a gradual slope. The highest penetration depth of GTAW using the 6 mm thick stainless steel plate is limited to 1.6 mm because of the heat-transfer and energy-transport characteristics of GTAW [16]. The graphs for the penetration depth of the F-GTA, PA and F-PA welds have steep slopes.

Full penetration of the F-GTAW, PAW and F-PAW joints was achieved by using welding currents greater than 185 A, 130 A and 115 A, respectively. The results of our study suggest that F-PAW offers a substantial advantage over F-GTAW in industrial applications that require high-current operations. Forming a welded joint using F-PAW can result in full penetration at relatively low welding current in a single-pass operation. Notably, a fully penetrated F-GTAW joint with a surface depression (Fig. 6) and a fully penetrated F-PAW joint with an undercut (Fig. 7) were generated using welding currents of 190 A and 130 A, respectively. The results signify that a high-current F-GTA weld is more susceptible to surface depression formation, while a high-current F-PA weld is more susceptible to undercut formation. The surface depression formed in the F-GTA weld and the undercut formed in the F-PA weld are respectively caused by the high arc pressure acting on the free surface of the welding pool and by the slowing of the backward flow of molten metal in the welding pool. Furthermore, surface depression formation caused an abnormal increase in both the bead width and penetration depth, while undercut formation caused an abnormal increase in bead width and decrease in penetration depth. Therefore, the joint penetration must be improved to maintain the integrity and soundness of the weld and thus to obtain a high-strength weldment through F-GTAW or F-PAW.

According to the experimental results described above, the dimensions of the welds could be substantially varied with and without using fluxes by varying the welding currents. When the welding current was increased from 120 A to 190 A, the bead width of the GTA weld increased from 6.31 mm to 11.03 mm, and the resultant penetration depth increased from 0.75 mm to 1.59 mm. The bead width of the F-GTA weld increased from 4.91 mm to 7.19 mm under the same current range, and the resultant penetration depth increased from 2.31 mm to 7.22 mm. Similarly, when the welding current was increased from 90 A to 130 A, the bead width of the PA weld increased from 6.58 mm to 7.53 mm, and the resultant penetration depth increased from 2.82 mm to 6.08 mm. The bead width of the F-PA weld increased from 5.42 mm to 6.08 mm under the same current range, and the resultant penetration depth increased from 3.09 mm to 6.56 mm. Fig. 8 shows the cross-sectional views of the weld profiles

Table 3
Physical properties of carrier solvent used in this study.

Physical properties	Carrier solvent		
	Water	Methanol	Acetone
Dynamic viscosity (mPa s)	0.89	0.54	0.31
Vapor pressure (kPa)	3.2	16.9	30.8

Table 4
Volatility of flux layer obtained with various single solvents (operating temperature of 26 ± 1 °C).

Single solvent	Evaporation time
100%W	1611 s
100%M	63 s
100%A	12 s

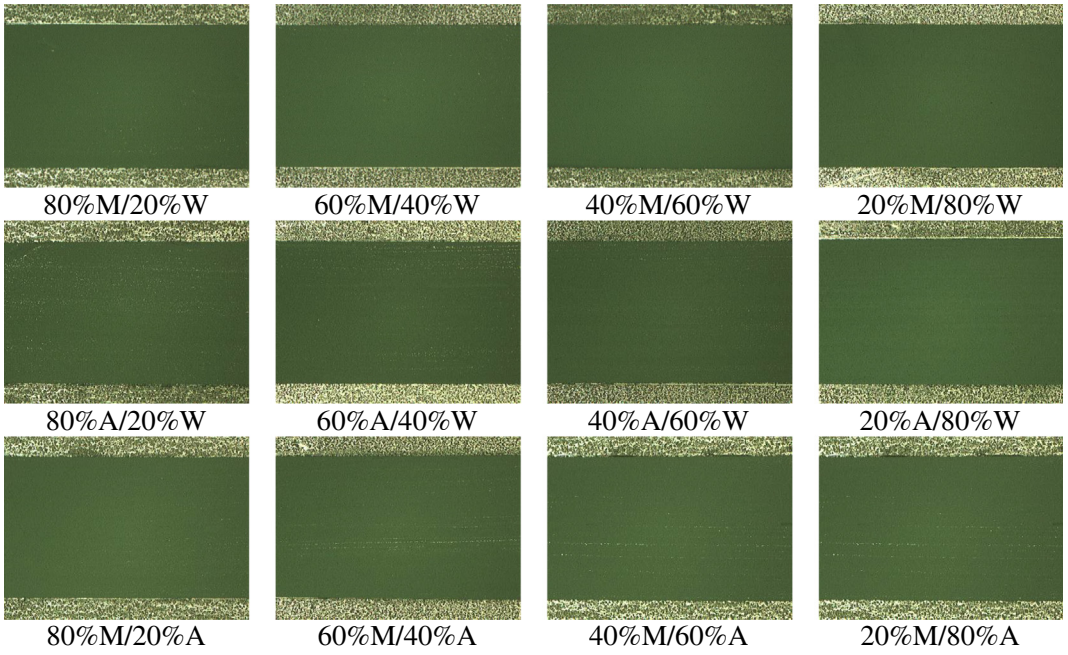

Fig. 3. Coverability of flux layer obtained with various multicomponent solvents.

made with and without the flux. In contrast to the GTA weld, which was wide and shallow (Fig. 8a), the F-GTA, PA and F-PA welds were deep and narrow (Fig. 8b–d). These observations indicate that F-GTAW produced a weld cross-sectional profile similar to that produced by PAW.

Fig. 9 shows the effect of the welding current on the reduction in bead width of the weld. Both the surface depression and undercut have significant effects on the bead width and penetration depth of the weld; therefore, experimental data for the surface depression and undercut welds were not considered as part of this investigation. Reduction in bead width (R_W) expressed as a percentage was calculated as follows:

$$R_W(\%) = \frac{W_{w/o} - W_{w/}}{W_{w/o}} \times 100\%$$

where $W_{w/o}$ is the bead width of the weld made without the flux; $W_{w/}$ is the bead width of the weld made with the flux.

When the F-GTAW current was increased from 120 A to 180 A, the reduction in bead width varied from 22.2% to 35.3%. The reduction in bead width for the F-PA weld remained at an average of 17.2% as the welding current was increased from 90 A to 120 A. This result implies that use of the flux cannot significantly decrease the bead width of both GTA and PA welds.

Fig. 10 shows the effect of the welding current on the increase in penetration depth of the weld. Increment in penetration depth (I_D) expressed as a percentage was calculated as follows:

$$I_D(\%) = \frac{D_{w/} - D_{w/o}}{D_{w/o}} \times 100\%$$

where $D_{w/o}$ is the penetration depth of the weld made without the flux; $D_{w/}$ is the penetration depth of the weld made with the flux.

When the F-GTAW current was increased from 120 A to 180 A, the increment in penetration depth increased from 208.0% to 304.8%. The increment in penetration depth for the F-PA weld varied from 9.6% to 14.2% as the welding current was increased from 90 A to 120 A. This result indicates that the use of the flux can significantly increase the penetration depth of the GTA weld. The influence of the flux on the geometry of the PA weld was not as pronounced as that on the geometry of the GTA weld. However, F-PAW produced a weld with a cross-sectional profile that is more uniform than that produced by PAW at the same current level.

3.4. Potential mechanism leading to the increase in joint-penetrating capability with use of the flux

Results of our study suggest that the joint penetration of grade 316 L stainless steel welds substantially changed because of the multicomponent flux. The joint-penetrating capability increase in F-AW could be explained in terms of mechanisms in the welding arc and the welding pool. In F-AW, the welding arc and the welding pool are characterized by the constricted plasma arc column and by the reversed molten metal convection, respectively [4]. Since the increments in the joint penetration of the weld occurring in the welding arc and the welding pool are coupled, they comprise a single integrated mechanism in F-AW.

Several mechanisms have been proposed to account for the observed increase in the joint penetration of the F-GTA weld. Each mechanism depends on the chemical composition of the flux and base metal, as well as the welding parameters [17]. Heiple and Roper [18]

Table 5
Volatility of flux layer obtained with various multicomponent solvents (operating temperature of 26 ± 1 °C).

Multicomponent solvent	Evaporation time	Multicomponent solvent	Evaporation time	Multicomponent solvent	Evaporation time
80%M/20%W	206 s	80%A/20%W	117 s	80%M/20%A	104 s
60%M/40%W	343 s	60%A/40%W	211 s	60%M/40%A	79 s
40%M/60%W	645 s	40%A/60%W	469 s	40%M/60%A	43 s
20%M/80%W	1019 s	20%A/80%W	763 s	20%M/80%A	21 s

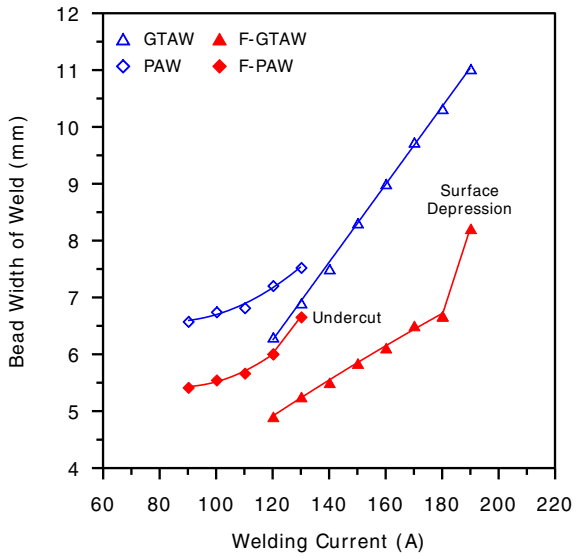

Fig. 4. Effect of welding current on bead width of weld.

stated that the presence of a certain amount of oxygen changes the sign of the surface tension temperature coefficient from negative to positive. This drives the convection of the molten metal from the edges toward the central region along the welding pool surface. Furthermore, Lu et al. [19] found that when the effective oxygen concentration in the austenitic stainless steel weld is between 70 ppm and 300 ppm, the surface tension of molten iron increases with increasing temperature; otherwise, the surface tension of decreases with increasing temperature. Lucas and Howse [12] stated that the vaporized flux molecules capture conduction electrons in the peripheral regions of the welding arc, thereby decreasing the number of conduction electrons in the peripheral regions of the welding arc. This decrease forces the welding arc to generate a higher energy state in the plasma arc column and produces a higher current density at the anode hotspot.

Fig. 11 shows the oxygen concentration in grade 316 L stainless steel welds made with and without the flux. The results indicate that the oxygen concentrations in grade 316 L stainless steel GTA and PA welds made without the flux were 37 ppm and 39 ppm, respectively. These concentrations suggest that insufficient dissolved oxygen was present in both grade 316 L stainless steel GTA and PA welds, resulting

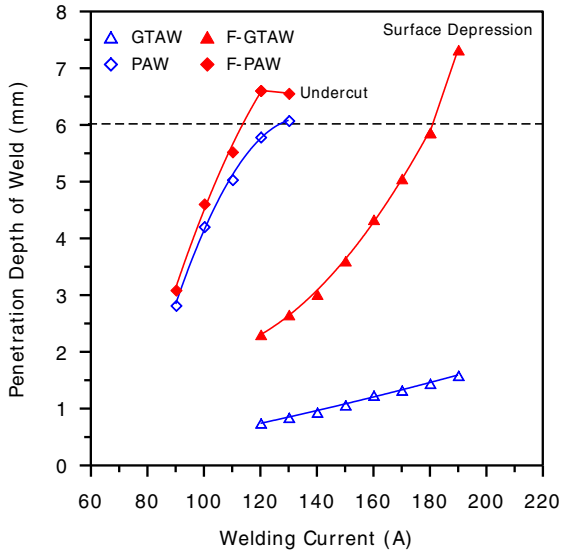

Fig. 5. Effect of welding current on penetration depth of weld.

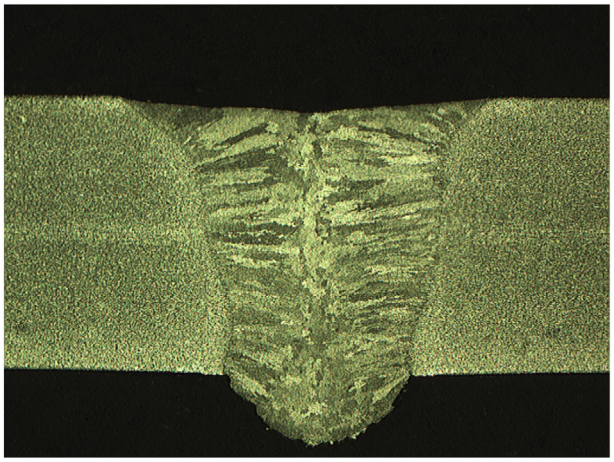

Fig. 6. F-GTA weld cross-sectional profile with surface depression (190 A/150 mm/min).

in an unchanged direction of the molten metal convection in the welding pool. Oxygen concentrations in grade 316 L stainless steel F-GTA and F-PA welds made with the flux were 87 ppm and 92 ppm, respectively. The increase in dissolved oxygen concentration in these welds was produced by the thermal decomposition of the multicomponent oxides. Therefore, both grade 316 L stainless steel F-GTA and F-PA welds had sufficient dissolved oxygen, which thus reversed the direction of the molten metal convection in the welding pool. Cross-sectional views of the welding arc contours made with and without the flux (Fig. 12) clearly show that the arc contour of the F-GTAW is smaller than that of the GTAW. This difference means that the plasma arc column of the F-GTAW is significantly constricted. However, the arc contours of both PAW and F-PAW were not markedly different; hence, the plasma arc column in PAW cannot be constricted more by using a flux.

The effect of the constricted plasma arc column coupled with the reversed molten metal convection led to an inward and downward fluid flow toward the bottom of the F-GTAW pool. This flow resulted in an effective heat energy transfer from the edges of the welding pool surface toward its center and subsequent downward transfer toward the bottom of the welding pool [20]. Consequently, F-GTAW substantially increased the joint-penetrating capability. In contrast, the use of the flux in PAW did not contribute to an increased physical constriction of the plasma arc column. This result implies that the action of the welding arc in the mechanism of the joint-penetrating capability increase in F-PAW is negligible. Thus, F-PAW did not produce a greater

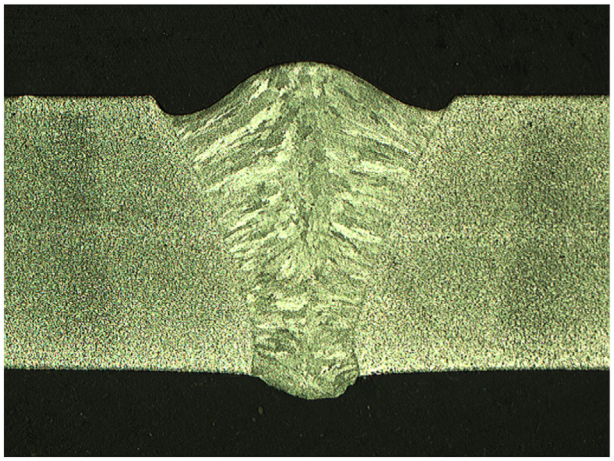

Fig. 7. F-PA weld cross-sectional profile with undercut (130 A/150 mm/min).

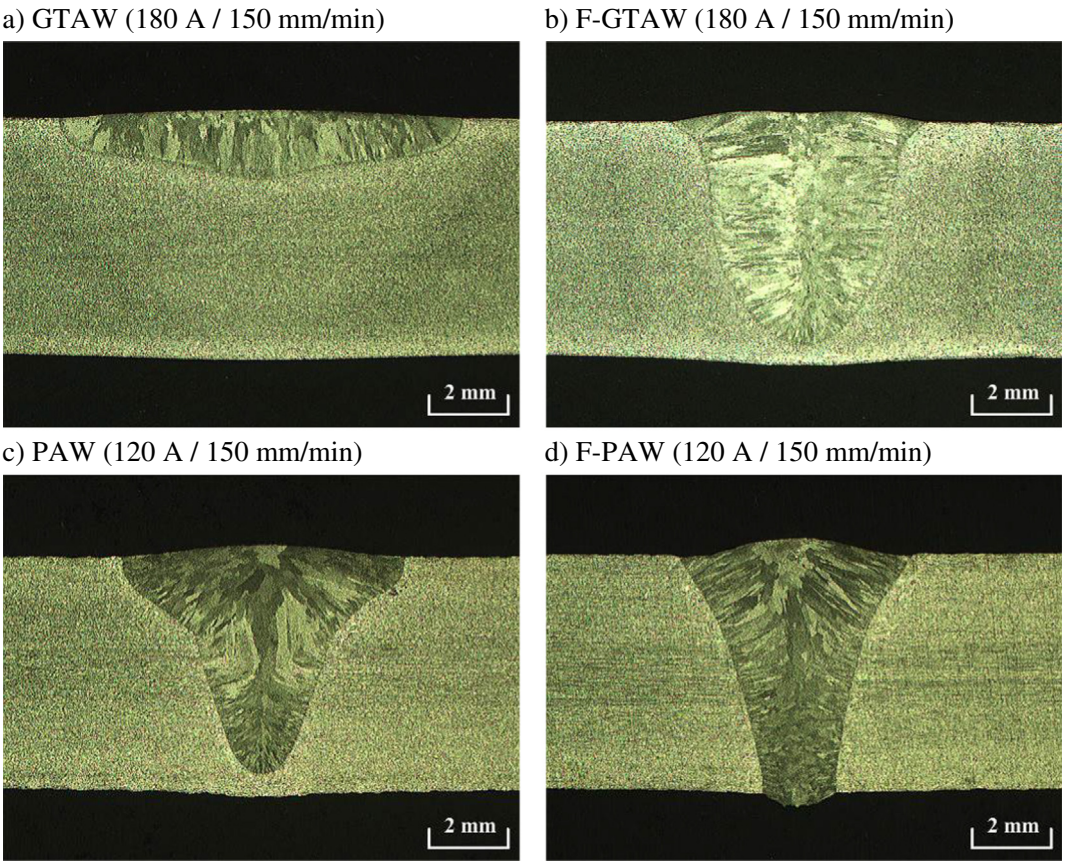

Fig. 8. Weld cross-sectional profiles made with and without flux.

increment in penetration depth. However, the use of the flux in PAW could contribute to an optimal geometry of the weld by reversing the direction of the molten metal convection in the welding pool, resulting in a more uniform cross-sectional profile of grade 316 L stainless steel F-PA weld compared with that of grade 316 L stainless steel PA weld.

Tseng and Hsu [21] found that changes in the arc voltage of F-AW reveal differences in the arc contour during welding. In arc welding using a constant-current power source, any variation in the arc length greatly affects the arc voltage. In the present work, an arc length controller was used to maintain a constant arc length during welding in order to prevent variations in the arc length from affecting the arc voltage. Fig. 13 shows the arc voltages of the welding processes with and without the flux. The results indicate that the arc voltages of both PAW and F-PAW are higher than those of both GTAW and F-GTAW, and that PAW and F-PAW therefore have greater arc energy concentration and arc stability in comparison with GTAW or F-GTAW. Compared with the arc voltage of GTAW at the same current level, that of F-GTAW was higher. However, the arc voltages of both PAW and F-PAW were not

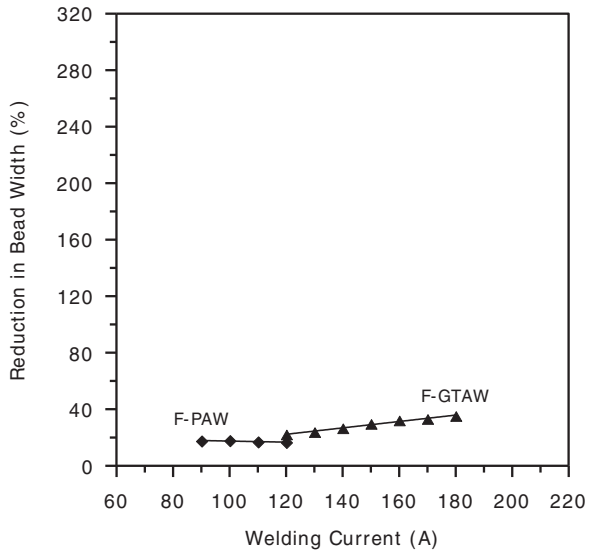

Fig. 9. Effect of welding current on reduction in bead width of weld.

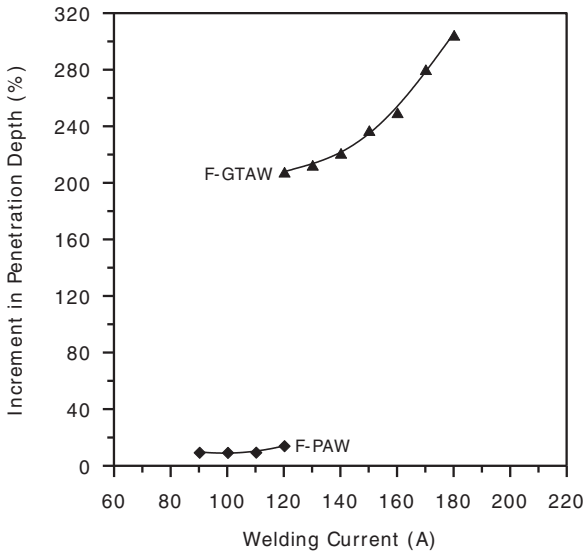

Fig. 10. Effect of welding current on increment in penetration depth of weld.

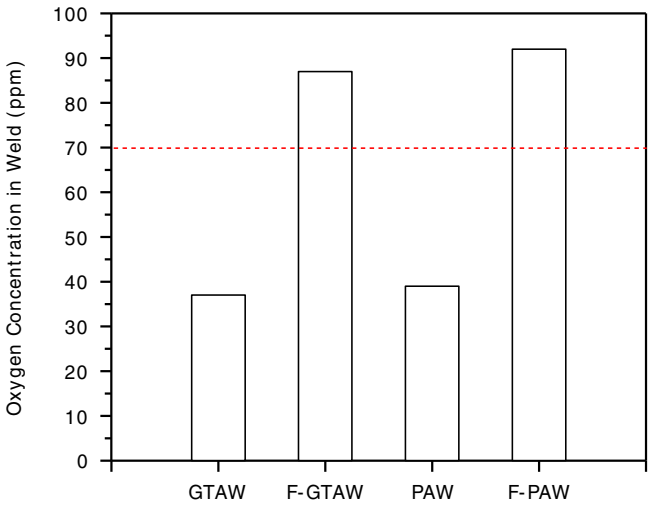

Fig. 11. Oxygen concentration in welds made with and without flux.

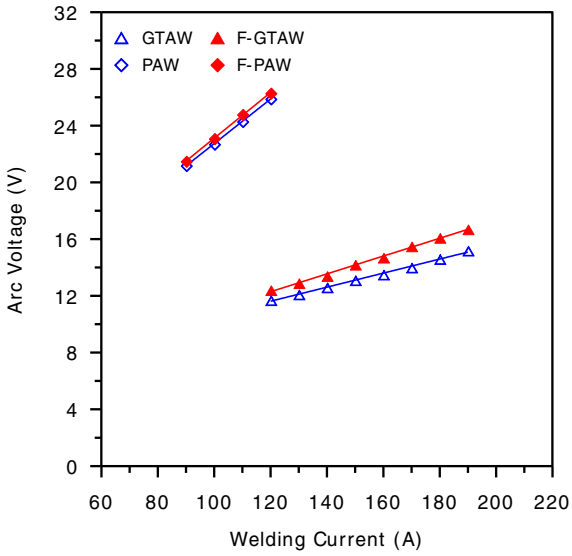

Fig. 13. Arc voltage of welding processes with and without flux.

markedly different. The measured arc voltage is strong evidence that the observed arc contour of F-GTAW is smaller than that of GTAW at the same current level and that the observed arc contours of both PAW and F-PAW are not very different from each other.

In F-AW, the ingredients of the flux are crucial to the geometry of the resultant weld. At present, very little information about the ingredients of the flux can be found in the open literature because of commercial reasons. The NPUST is currently carrying out empirical investigations on the use of the fluxes in arc welding as part of its core research program. The results of our study suggest that a 30% SiO_2, 25% TiO_2, 20% ZnO, 12% NiO, 5% MgO, 3% Cu_2O and 5% FeF_2 flux not only significantly improves the joint penetration of a GTA weld, but it also leads to a more uniform cross-sectional profile of the PA weld. Our study also increased understanding of the characteristics of multicomponent fluxes in terms of their effects on the joint penetration of both GTA and PA welds. It may therefore contribute to the development of new multicomponent fluxes used in stainless steel arc welding for a wide range of industrial applications.

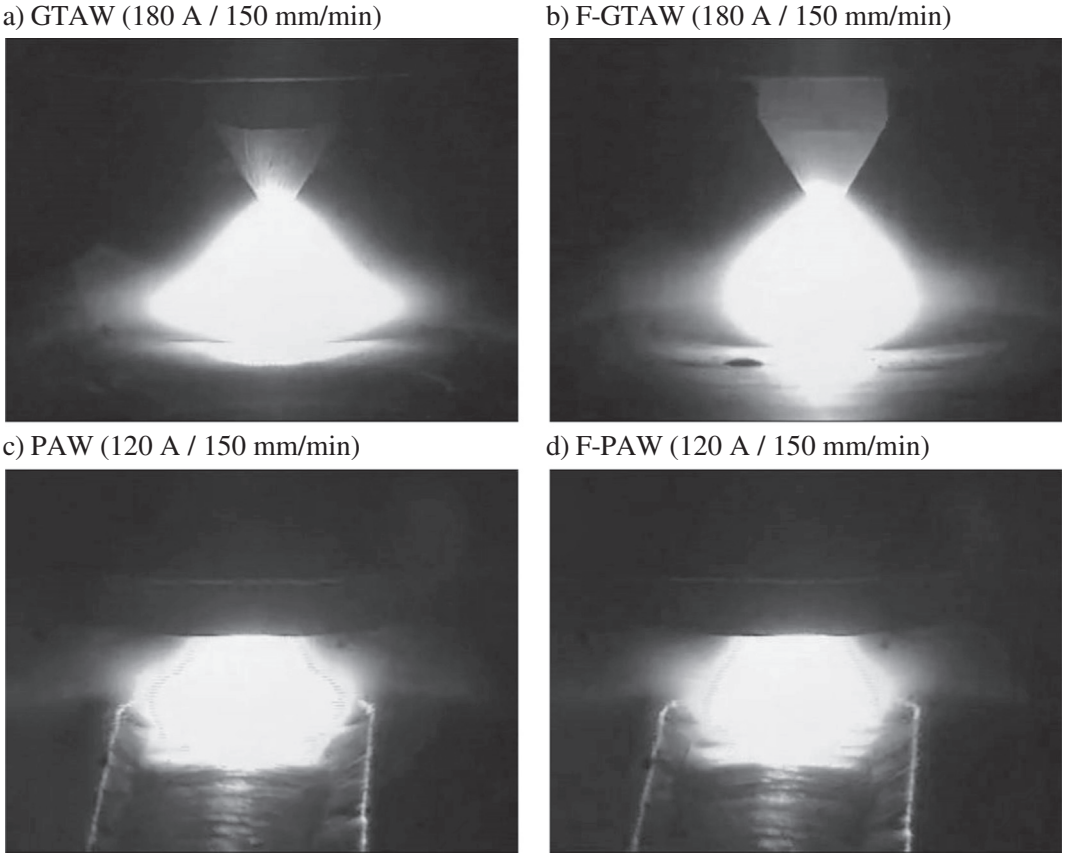

Fig. 12. Welding arc contours made with and without flux.

4. Conclusions

This study has clearly demonstrated the potential benefits of GTAW and PAW of grade 316 L stainless steel assisted by a multicomponent flux developed by the NPUST. The integrated mechanisms behind the increase in joint-penetrating capability in F-GTAW and F-PAW are discussed. The effects of carrier solvents on the coverability and volatility of the flux layers were also investigated. The main conclusions from this study are as follows:

1. A single solvent cannot be used to produce a flux layer with good coatability. A 60% methanol/40% water or a 40% acetone/60% water is an appropriate solvent mixture for mixing with the multicomponent powders.
2. High-current F-GTA and F-PA welds are more susceptible to surface depression formation and undercut formation, respectively. The joint penetration must therefore be improved to maintain the integrity and soundness of the weld and to obtain a high-strength weldment through F-GTAW or F-PAW.
3. In contrast to the GTA weld, which is shallow and wide, the F-GTA, PA and F-PA welds are deep and narrow. F-GTAW produces a weld with a cross-sectional profile similar to that produced by PAW.
4. In F-GTAW, the effect of the constricted plasma arc column coupled with the reversed molten metal convection leads to a significant increase in joint-penetrating capability.
5. The use of the flux in PAW does not contribute to a significant physical constriction of the plasma arc column. Thus, F-PAW does not produce a greater improve in joint-penetrating capability. However, the use of the flux in PAW may contribute to an optimal geometry of the weld by reversing the direction of the molten metal convection in the welding pool. This reversal results in a more uniform cross-sectional profile of the F-PA weld compared with that of the PA weld.
6. A 30% SiO_2, 25% TiO_2, 20% ZnO, 12% NiO, 5% MgO, 3% Cu_2O and 5% FeF_2 flux not only significantly improves the joint penetration of the GTA weld, but it also produces a PA weld with a more uniform cross-sectional profile.

Acknowledgments

The authors gratefully acknowledge the financial support provided to this study by the Ministry of Science and Technology, Taiwan under grant no. 104-2221-E-020-034.

References

[1] H.Y. Huang, Research on the activating flux gas tungsten arc welding and plasma arc welding for stainless steel, Met. Mater. Int. 16 (2010) 819–825.
[2] J.N. DuPont, A.R. Marder, Thermal efficiency of arc welding processes, Weld. J. 74 (1995) 406–416.
[3] K.H. Tseng, S.T. Hsieh, C.C. Tseng, Effect of process parameters of micro-plasma arc welding on morphology and quality in stainless steel edge joint welds, Sci. Technol. Weld. Join. 8 (2003) 423–430.
[4] K.H. Tseng, P.Y. Lin, UNS S31603 stainless steel tungsten inert gas welds made with microparticle and nanoparticle oxides, Materials 7 (2014) 4755–4772.
[5] B. Arivazhagan, M. Vasudevan, Studies on A-TIG welding of 2.25Cr—1Mo (P22) steel, J. Manuf. Process. 18 (2015) 55–59.
[6] K.H. Tseng, Development and application of oxide-based flux powder for tungsten inert gas welding of austenitic stainless steels, Powder Technol. 233 (2013) 72–79.
[7] K.D. Ramkumar, P.S. Goutham, V.S. Radhakrishna, A. Tiwari, S. Anirudh, Studies on the structure-property relationships and corrosion behaviour of the activated flux TIG welding of UNS S32750, J. Manuf. Process. 23 (2016) 231–241.
[8] T. Sándor, C. Mekler, J. Dobránszky, G. Kaptay, An improved theoretical model for A-TIG welding based on surface phase transition and reversed Marangoni flow, Metall. Mater. Trans. A 44 (2013) 351–361.
[9] K.H. Tseng, Study on surface appearance, geometry size, and delta-ferrite content of ZrO_2-aided TIG welding of AISI 316LN stainless steel, Int. J. Adv. Manuf. Technol. (2016)http://dx.doi.org/10.1007/s00170-016-9280-2.
[10] K.H. Tseng, K.J. Chuang, Application of iron-based powders in tungsten inert gas welding for 17Cr—10Ni—2Mo alloys, Powder Technol. 228 (2012) 36–46.
[11] K.H. Tseng, C.S. Chen, Characteristics of nanoscale active oxide in enhancing penetration capability of surfactant flux assisted TIG welding, J. Nanosci. Nanotechnol. 17 (2017) 1796–1805.
[12] W. Lucas, D. Howse, Activating flux-increasing the performance and productivity of the TIG and plasma processes, Weld. Met. Fabr. 64 (1996) 11–17.
[13] O.M. Savytsky, M.M. Savytsky, Y.M. Shkrabalyuk, T. Vuherer, D.R. Bajić, The influence of electric arc activation on the speed of heating and the structure of metal in welds, Therm. Sci. 20 (2016) 239–246.
[14] K.H. Tseng, Y.J. Shiu, Effect of thermal stability of powdered oxide on joint penetration and metallurgical feature of AISI 4130 steel TIG weldment, Powder Technol. 286 (2015) 31–38.
[15] P.J. Modenesi, E.R. Apolinário, I.M. Pereira, TIG welding with single-component fluxes, J. Mater. Process. Technol. 99 (2000) 260–265.
[16] K.H. Tseng, N.S. Wang, GTA welding assisted by mixed ionic compounds of stainless steel, Powder Technol. 251 (2014) 52–60.
[17] M. Marya, G.R. Edwards, Chloride contributions in flux-assisted GTA welding of magnesium alloys, Weld. J. 81 (2002) 291–298.
[18] C.R. Heiple, J.R. Roper, Mechanism for minor element effect on GTA fusion zone geometry, Weld. J. 61 (1982) 97–102.
[19] S.P. Lu, H. Fujii, H. Sugiyama, K. Nogi, Mechanism and optimization of oxide fluxes for deep penetration in gas tungsten arc welding, Metall. Mater. Trans. A 34 (2003) 1901–1907.
[20] K.H. Tseng, P.Y. Chen, Effect of TiO_2 crystalline phase on performance of flux assisted GTA welds, Mater. Manuf. Process. 31 (2016) 359–365.
[21] K.H. Tseng, C.Y. Hsu, Performance of activated TIG process in austenitic stainless steel welds, J. Mater. Process. Technol. 211 (2011) 503–512.